

# Numerical investigation of laminar flow and heat transfer of non-Newtonian nanofluid within a porous medium



Pouya Barnoon, Davood Toghraie \*

Department of Mechanical Engineering, Khomeinishahr Branch, Islamic Azad University, Khomeinishahr, Iran

## ARTICLE INFO

### Article history:

Received 9 August 2017

Received in revised form 19 September 2017

Accepted 19 October 2017

Available online xxxx

### Keywords:

Laminar flow

Heat transfer

Non-Newtonian nanofluid

Porous

## ABSTRACT

In this study, comprehensive study of laminar flow and heat transfer of pseudo-plastic non-Newtonian nanofluid ( $\text{Al}_2\text{O}_3 + \text{CMC}$ ) within the porous circular concentric region is presented. The effect of volume fraction of nanoparticles, Reynolds number, Darcy number, thickness ratio is studied. Simulations for different Reynolds numbers and Darcy numbers in the range of  $100 \leq \text{Re} \leq 300$  and  $10^{-4} \leq \text{Da} \leq 10^{-2}$  are done. The results show that the effect of the porous layer on increasing the convective heat transfer coefficient is larger than the Reynolds number, since, at a given volume fraction, the porous medium plays a greater role in increasing the heat transfer compared to the increasing Reynolds number. Also, at a given volume fraction and for a fixed porosity, decreases in the permeability leads to increased Darcy velocity and, consequently, velocity profile. As the thickness of the porous layer increases at fixed values of permeability and porosity, the velocity of the nanofluid is also increased in a constant Reynolds number, by increasing the thickness of the porous media, heat transfer coefficient increases. In addition, at a specified thickness and constant Reynolds number, by increasing the Darcy number, the heat transfer coefficient and the Nusselt number increases. Moreover, as the thickness of the porous layer increases at fixed values of permeability and porosity, the velocity of the nanofluid is also increased; this consequently maximizes the pressure drop.

© 2017 Elsevier B.V. All rights reserved.

## 1. Introduction

A non-Newtonian fluid is a fluid that does not follow Newton's law of viscosity. Shear thinning is the non-Newtonian behavior of fluids whose viscosity decreases under shear strain [1,2]. In fluid mechanics, fluid flow through porous media is the manner in which fluids behave when flowing through a porous medium. The concept of porous media is used in many areas of applied science and engineering [3]. Nanofluids are fluids containing nanoparticles. They are engineered colloidal suspensions of nanoparticles in a base fluid. They exhibit enhanced thermal conductivity and the convective heat transfer coefficient compared to the base fluid [4–13].

Hatami and Ganji [14] analyzed heat transfer and flow for non-Newtonian nanofluid passing through the porous media between two coaxial cylinders. They showed that increasing the thermophoresis parameter caused an increase in temperature values in whole domain.

Nield and Kuznetsov [15] studied the forced convection in a channel occupied by a nanofluid or a porous medium saturated by a nanofluid. They found that the combination of Brownian motion and thermophoresis has the effect of reducing the Nusselt number.

Uphill et al. [16] investigated flow of nanofluids through porous media. They showed that nanofluids containing particles smaller than 60 nm flowed well through timber.

Bourantas et al. [17] studied heat transfer and natural convection of nanofluids in porous media. They found that higher Rayleigh number values strengthen the natural convection flows.

Sheremet and Pop [18] investigated the potential of nanofluids to enhance the heat transfer rate due to natural convection in a porous annulus. Their findings showed that Brownian motion parameter has the minimum influence on Nusselt number.

Mahdi et al. [19] reviewed heat transfer and fluid flow in porous media with nanofluid. They investigated the effects of several parameters in porous media geometry and thermophysical properties of nanofluid, thermal boundary conditions and types of nanofluids.

Kefayati [20] studied heat transfer and entropy generation of natural convection on non-Newtonian nanofluids in a porous cavity. He concluded that the addition of the nanoparticle enhances the average Nusselt number.

Sivasankaran and Narrein [21] investigated the two-phase laminar pulsating nanofluid flow in helical microchannel filled with a porous medium. They observed that the presence of porous media led to improvement in heat transfer performance.

Ghalambaz et al. [22] studied free convection in a square cavity filled by a porous medium saturated by a nanofluid. They concluded that the

\* Corresponding author.

E-mail address: [davoodtoghraie@gmail.com](mailto:davoodtoghraie@gmail.com) (D. Toghraie).

**Nomenclature**

|                               |   |
|-------------------------------|---|
| Re                            | Reynolds number   |
| T                             | temperature (K)   |
| U                             | dimensionless velocity  |
| <i>Greek symbols</i>          |   |
| $\varepsilon$                 | porosity  |
| $\varphi$                     | volume fraction   |
| $\rho$                        | density [ $\text{kg}/\text{m}^3$ ]                                  |
| <i>Super- and sub-scripts</i> |   |
| f                             | fluid   |
| nf                            | nanofluid   |
| p                             | particle  |
| bf                            | base fluid  |
| s                             | solid   |
| ave                           | average   |
| o                             | outer   |
| i                             | inner   |
| $C_p$                         | specific heat capacity [ $\text{J}/\text{kg}\cdot\text{K}$ ]        |
| Da                            | Darcy number  |
| f                             | friction factor   |
| $f_s$                         | friction factor in smooth pipe                                      |
| h                             | heat transfer coefficient [ $\text{W}/\text{m}^2\cdot\text{K}$ ]    |
| $D_i$                         | inner diameter [m]  |
| $D_o$                         | outer diameter [m]  |
| K                             | consistency index [ $\text{Pa}\cdot\text{s}^n$ ]                    |
| k                             | thermal conductivity [ $\text{W}/\text{m}\cdot\text{K}$ ]           |
| $K^{**}$                      | permeability [ $\text{m}^2$ ]                                       |
| $K^*$                         | modified permeability [ $\text{m}^{n+1}$ ]                          |
| $k_{\text{eff}}$              | effective thermal conductivity [ $\text{W}/\text{m}\cdot\text{K}$ ] |
| L                             | length [m]  |
| Nu                            | Nusselt number  |
| $\text{Nu}_s$                 | Nusselt number in smooth pipe                                       |
| n                             | power law index   |
| Pr                            | Prandtl number  |

increase of Lewis number and buoyancy ratio parameter, respectively, increases and decreases the average Nusselt number.

Devakar et al. [23] simulated fully developed flow of non-Newtonian fluids in a straight uniform square duct through porous medium. They observed that, the velocity and volume flow rate decrease with an increase in couple stress parameter and porosity parameter.

Kasaean et al. [24] reviewed the latest developments Nanofluid flow and heat transfer in porous media. They found that Tiwari and Das, and Buongiorno models were the most popular models used to simulate the nanofluid flow in porous media.

Selimefendigil et al. [25] simulated mixed convection in superposed nanofluid and porous layers in square enclosure. They found that the averaged heat transfer enhances almost linearly with nanoparticle volume fraction for different cylinder sizes.

Solomon et al. [26] investigated natural convection enhancement in a porous cavity with  $\text{Al}_2\text{O}_3$ -Ethylene glycol/Water nanofluids. They found that at a volume concentration of 0.05%, the heat transfer capability of porous cavity is enhanced to a maximum of 10% compared to the base fluids.

Reddy et al. [27] investigated boundary layer flow, heat and mass transfer over a rotating disk through porous medium saturated by Cu-Water and Ag-Water nanofluid with chemical reaction. They concluded that the temperature profiles elevated with the increasing values of nanoparticle volume fraction parameter.

Hashemi et al. [28] studied natural convection within a porous enclosure occupied by Cu-Water micropolar nanofluid at the presence of the heat generated in both solid and fluid phases of the porous medium. They found that as external Darcy-Rayleigh number increases, the strength of vortices formed and micro-rotation of particles increases.

Aly [29] studied natural convection over circular cylinders in a porous enclosure filled with a nanofluid under thermo-diffusion effects. He found that, the size and formation of cells inside the enclosure strongly depend on the Rayleigh number with Darcy parameter, and sizes and locations of the inner circular cylinders.

The present study includes three key elements: nanofluid, non-Newtonian fluid, and porous medium. In this study, comprehensive study of laminar flow and heat transfer of pseudo-plastic non-Newtonian nanofluid ( $\text{Al}_2\text{O}_3 + \text{CMC}$ ) within the porous circular concentric region is presented.

**2. Statement of the problem**

Comprehensive study of laminar flow and heat transfer of pseudo-plastic non-Newtonian nanofluid ( $\text{Al}_2\text{O}_3 + \text{CMC}$  (0.5% wt)) within the porous circular concentric region is investigated numerically by using of finite volume method. The schematic of the problem in this study is shown in Fig. 1. The channel length  $L = 3$  m, the outer diameter is  $D_o = 5$  cm and inner diameter is  $D_i = 4$  cm. The walls of the channel are under a constant flux of  $q'' = 6000 \text{ W}/\text{m}^2$ . The inlet temperature of the nanofluid is  $T_{\text{in}} = 298$  K. Water and  $\text{Al}_2\text{O}_3$  nanoparticles (particle diameter 20 nm) are in thermal equilibrium. The Reynolds and Darcy numbers ranges are  $100 < Re < 300$  and  $10^{-4} < Da < 10^{-2}$ . The intended range for  $\text{Al}_2\text{O}_3$  nanoparticles volume fraction has been selected by Hojjat et al. [33]. The minimum volume fraction considered in their paper was 0% and the maximum volume fraction was 1.5%. So, In this study the volume fraction of the nanoparticles is  $\varphi = 1\text{--}1.5\%$  and the porous layer thickness range is  $0 \geq R_p \geq 0.6$ ,

**3. Governing equations**

In this study, a single-phase model has been considered to analyze heat transfer and the flow of the non-Newtonian nanofluid within the porous circular concentric region. The resulting equations over the fluid flow include equations of conservation of mass, momentum and energy.

*Continuity equation:*

$$\rho_{\text{nf}} \left( \frac{1}{r} \left( \frac{\partial(ru_r)}{\partial r} \right) + \frac{1}{r} \left( \frac{\partial u_\theta}{\partial \theta} \right) + \left( \frac{\partial u_z}{\partial z} \right) \right) = 0 \quad (1)$$

*Momentum equations:*

$$\begin{aligned} \rho_{\text{nf}} \left( u_r \frac{\partial u_r}{\partial r} + \frac{V_\theta}{r} \frac{\partial u_r}{\partial \theta} - \frac{u_\theta^2}{r} + u_z \frac{\partial u_r}{\partial z} \right) \\ = - \frac{\partial P}{\partial r} + \eta \left[ \frac{1}{r} \frac{\partial}{\partial r} \left( r \frac{\partial u_r}{\partial r} \right) - \frac{u_r}{r^2} + \frac{1}{r^2} \frac{\partial^2 u_r}{\partial \theta^2} - \frac{2}{r^2} \frac{\partial u_\theta}{\partial \theta} + \frac{\partial^2 u_r}{\partial z^2} \right] + S_r \end{aligned} \quad (2)$$

$$\begin{aligned} \rho_{\text{nf}} \left( u_r \frac{\partial u_\theta}{\partial r} + \frac{u_\theta}{r} \frac{\partial u_\theta}{\partial \theta} + \frac{u_\theta u_r}{r} + u_z \frac{\partial u_\theta}{\partial z} \right) \\ = - \frac{1}{r} \frac{\partial P}{\partial \theta} + \eta \left[ \frac{1}{r} \frac{\partial}{\partial r} \left( r \frac{\partial u_\theta}{\partial r} \right) - \frac{u_\theta}{r^2} + \frac{1}{r^2} \frac{\partial^2 u_\theta}{\partial \theta^2} + \frac{2}{r^2} \frac{\partial u_r}{\partial \theta} + \frac{\partial^2 u_\theta}{\partial z^2} \right] + S_\theta \end{aligned} \quad (3)$$

$$\begin{aligned} \rho_{\text{nf}} \left( u_r \frac{\partial u_z}{\partial r} + \frac{u_\theta}{r} \frac{\partial u_z}{\partial \theta} + u_z \frac{\partial u_z}{\partial z} \right) \\ = - \frac{\partial P}{\partial z} + \eta \left[ \frac{1}{r} \frac{\partial}{\partial r} \left( r \frac{\partial u_z}{\partial r} \right) + \frac{1}{r^2} \frac{\partial^2 u_z}{\partial \theta^2} + \frac{\partial^2 u_z}{\partial z^2} \right] + S_z \end{aligned} \quad (4)$$

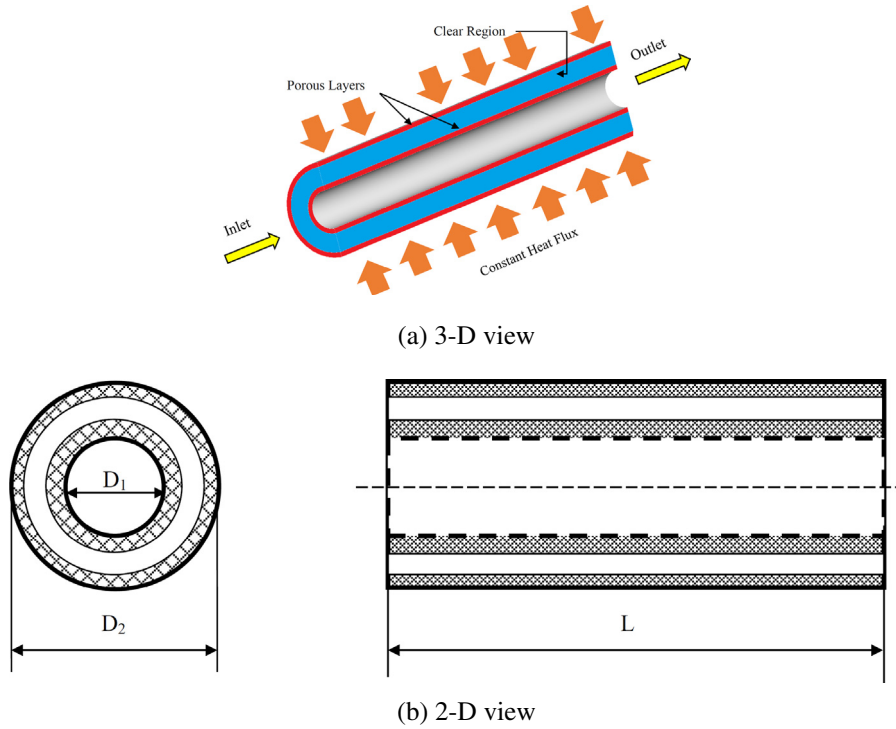


Fig. 1. Schematic of the problem.

Energy equation:

$$\nabla \cdot (\rho_{nf} \mathbf{u}_i (C_p)_{nf} T) = \nabla \cdot [k_{eff} \nabla T - (\sum_i h_i J_i) + (\bar{\tau} \cdot \nabla)] \quad (5)$$

The speculation of the dynamic viscosity behavior of the flow in the numerical solution field is analyzed using the non-Newtonian power-law method in which the viscosity is defined as,

$$\eta = K(\dot{\gamma})^{n-1} \quad (6)$$

In this equation,  $K$ ,  $\dot{\gamma}$  and  $n$  are respectively consistency index, shear rate and power-law index. Also, in the momentum equation we have,

$$S_r = -\left(\frac{\eta}{K^{**}} u_r + C \frac{1}{2} \rho |\bar{\mathbf{u}}| u_r\right) \quad (7-a)$$

$$S_\theta = -\left(\frac{\eta}{K^{**}} u_\theta + C \frac{1}{2} \rho |\bar{\mathbf{u}}| u_\theta\right) \quad (7-b)$$

$$S_z = -\left(\frac{\eta}{K^{**}} u_z + C \frac{1}{2} \rho |\bar{\mathbf{u}}| u_z\right) \quad (7-c)$$

And, in the energy equation we have,

$$\bar{\tau} = \eta(\bar{\mathbf{D}}) \bar{\mathbf{D}} \quad (8)$$

where,

$$\bar{\mathbf{D}} = \left( \frac{\partial u_j}{\partial x_i} + \frac{\partial u_i}{\partial x_j} \right) \quad (9)$$

$k_{eff}$  of porous material is obtained from the following equations,

$$k_{eff} = \varepsilon k_{nf} + (1-\varepsilon)k_s \quad (10)$$

For calculating the density of nanofluid and the specific heat capacity, the following equations are used [30,31]

$$\rho_{nf} = \varphi \rho_p + (1-\varphi) \rho_f \quad (11)$$

$$(\rho C_p)_{nf} = \varphi (\rho C_p)_p + (1-\varphi) (\rho C_p)_f \quad (12)$$

In the above equations,  $\varphi$  is the volume fraction of nanoparticle and  $f$ ,  $p$  and  $nf$  indexes are respectively the indicators of fluid, solid and nanofluid. In order to determine the thermal conductivity of nanofluid, the following equations [32,33] are used. Moreover, since the base fluid was non-Newtonian, instead of determining viscosity, values of  $n$  and  $K$  at 25 °C were used for the aluminum oxide nanofluid by Hojjat et al. [33]. Given that  $n < 1$ , the non-Newtonian fluid is pseudoplastic. The thermo-physical of  $Al_2O_3$  nanoparticle and base fluid are shown in Table 1 [94].

In order to describe Reynolds and Prandtl numbers for the non-Newtonian fluid, coefficient index and power-law index are very important in determining Reynolds number and initial velocity of fluid in the inlet of tube. Reynolds and Prandtl numbers are described for the non-Newtonian fluid as follow [33],

$$Re = \frac{\rho u^{2-n} D_h^n}{K} \quad (13)$$

$$Pr = \frac{C_p K \left(\frac{u}{D_h}\right)^{n-1}}{k} \quad (14)$$

**Table 1**  
Thermophysical properties of the base fluid and  $Al_2O_3$  nanoparticles [94].

|                    | $\rho$ ( $kg/m^3$ ) | $C_p$ ( $J/kgK$ ) | $k$ ( $W/mK$ ) |
|--------------------|---------------------|-------------------|----------------|
| Water + CMC (%0.5) | 998.2               | 4182              | 0.6            |
| $Al_2O_3$          | 3880                | 773               | 36             |

Darcy number is described for the non-Newtonian fluid as follow [98],

$$Da = \frac{\left(\frac{K^*}{\varepsilon^n}\right)^{\frac{2}{1+n}}}{D_h^2} \quad (15)$$

In this equation, n and K\* are respectively power-law index and modified consistency index [34]. K\* is defined such as follows,

$$K^* = \frac{1}{2c_t} \left(\frac{n\varepsilon}{3n+1}\right)^n \left(\frac{50K^{**}}{3\varepsilon}\right) \quad (16)$$

where K\*\* is permeability and c<sub>t</sub> is defined such as follows [34],

$$c_t = 2.5^n \times 2^{\left(\frac{1-n}{2}\right)} \quad (17)$$

Reynolds number in porous media is define such as follows [34],

$$Re_{Porous} = \frac{\rho \left(\frac{K^{**}}{\varepsilon}\right)^{n/2} \left(\frac{u}{\varepsilon}\right)^{2-n}}{K} \quad (18)$$

where ε is porosity coefficient and K\*\* is permeability. The local heat transfer coefficient is defined as [35],

$$h(x) = \frac{q''}{T_w(x) - T_b(x)} \quad (19)$$

where q'' = 6000  $\frac{W}{m^2}$  is the surface heat flux. Where T<sub>b</sub>(x) and T<sub>w</sub>(x) is the bulk temperature of the fluid passing the channel at cross-section x and wall temperature, respectively [36],

$$T_b(x) = \frac{\int T\rho|\vec{u}\cdot d\vec{A}|}{\int \rho|\vec{u}\cdot d\vec{A}|} \quad (20)$$

$$T_w(x) = \frac{1}{A} \int TdA \quad (21)$$

where A is cross section area, T is temperature profile, ρ<sub>nf</sub> is the nanofluid density and u is the velocity profile. For calculating the local Nusselt number, following equation is used [35],

$$Nu(x) = \frac{h(x)D_h}{k_{nf}} \quad (22)$$

where D<sub>h</sub> is the hydraulic diameter and is the thermal conductivity of nanofluid. Hydraulic diameter is defined such as follows [35],

$$D_h = \frac{4\left(\frac{\pi}{4}\right)(D_o^2 - D_i^2)}{\pi D_o + \pi D_i} = D_o - D_i \quad (23)$$

In laminar flow the pressure drop is typically proportional to velocity, the Darcy's law for porous media is obtained from the following equation,

$$\nabla P = -\frac{\eta}{K^{**}} \vec{u} \quad (24)$$

Hence, the pressure drop is expressed such as follow [36,37],

$$\Delta P = f \frac{L\rho u_{in}^2}{2D_h} \quad \text{for clear region} \quad (25)$$

$$\frac{\Delta P}{L} = \frac{150\eta}{D_p^2} \frac{1-\varepsilon^2}{\varepsilon^3} u_{in} \quad \text{for porous region} \quad (26)$$

where, L is the length of porous media, u<sub>in</sub> is inlet velocity, D<sub>p</sub> is average diameter of porous media and ε is porosity. Finally, we have,

$$\Delta P_T = \frac{1}{A} \int \Delta PdA \quad (27)$$

Non-dimensional velocity is defined such as follows,

$$U = \frac{u}{u_{in}} \quad (28)$$

where u<sub>in</sub> is the inlet velocity. Non-dimensional thickness of porous layer is defined as follows,

$$R_p = \frac{r_p}{r'} \quad (29)$$

where,

$$r_p = r_{p1} + r_{p2} \quad (30)$$

where r<sub>p1</sub> and r<sub>p2</sub> are half-thickness of porous layer in outer and inner tubes. Also, r' is half distance between two tubes. R is defined such as follows,

$$R = \frac{r}{r_0} \quad (31)$$

where r<sub>0</sub> is radial component and is outer radius of tube. Non-dimensional temperature is defined such as follows,

$$\theta = \frac{T - T_C}{T_H - T_C} \quad (32)$$

where T<sub>H</sub> and T<sub>C</sub> are hot and cold temperatures, respectively.

### 3.1. Thermophysical properties

In this study, Eqs. 11 and 12 were used to determine the density and specific heat capacity of nanofluids, respectively. Thermal conductivity of nanofluid is obtained from [32].

### 3.2. Solution procedure

The numerical simulation of this study has been done by using of finite volume method, which includes the following,

- a) Divide the domain into separate control volumes by using a computational grid.
- b) Integrating equations in each control volume to generate algebraic equations or dependent variables such as velocity, pressure and temperature.
- c) Linearization of independent equations and solving this system of equations in order to achieve new values of dependent variables.

Since the governing equations are not linear, several iteration in the solving loop must be done before convergent solution would obtained. Fig. 2 illustrates the method of solving the governing equations. For simulating the numerical solution, the coupled velocity and pressure equation, are used. In this method, coupled systems including mass conservation and momentum equations are solved. Due to the simultaneous solution of continuity and momentum equations, the convergent amount, comparing to the other methods, increases significantly. However, the demanded memory for solution enhances, because in this method, for calculating the pressure and velocity, all variables and parameters of momentum and continuity stored in memory, for obtaining the efficiency in the numerical solution, discrediting the second order upwind and SIMPLEC algorithm [38] and non-Newtonian power-law method are considered. In all of the defined states, for different Reynolds numbers and volume

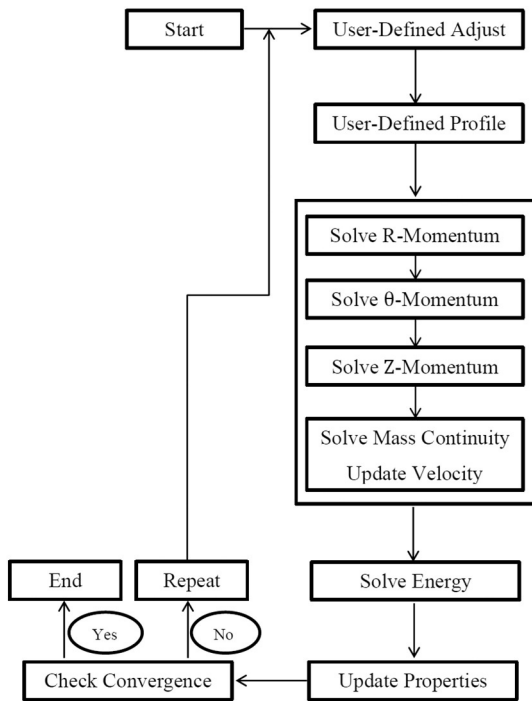


Fig. 2. The method of solving the governing equations.

fractions, in order to less use of computer memory and consuming in the numerical procedure, the maximum remaining of  $10^{-6}$  has been used.

### 3.3. Grid independency

In order to investigate the effect of number of cells on the computational grid, four types of grids were generated so that one can finally be selected for the solution. The parameters of Nusselt number and dynamic pressure were considered as the stability criterion for the solutions of the problem. Tables 2 and 3 present the results of grid independency for the thickness ratio and volume fraction of 0.2 and 1.5% at a  $Re = 100$ , respectively. As demonstrated, since the variation in the Nusselt number is small switching from grid 3 to grid 4, the former was considered as the appropriate grid for the entire process.

### 3.4. Validation

The present study includes three key elements: nanofluid, non-Newtonian fluid, and porous medium. In order to validate the employed numerical method, the result of the present study was compared to those of different references. According to the results, the results were in good agreement with the three considered references [35,38, and 39]. In the initial stage, the values of Nusselt numbers are compared by considering no porous medium and solving the problem with Water as the fluid. According to [35], in the case of two inner and outer concentric annular

surfaces subject to constant heat flux, the Nusselt number is calculated as follows:

$$Nu_i = \frac{Nu_{ii}}{1 - \left(\frac{q_o}{q_i}\right) \theta_i^*} \quad (33)$$

$$Nu_o = \frac{Nu_{oo}}{1 - \left(\frac{q_i}{q_o}\right) \theta_o^*} \quad (34)$$

Given  $D_i/D_o = 0.8$ , the values of  $Nu_{ii}$ ,  $Nu_{oo}$ ,  $\theta_i^*$ , and  $\theta_o^*$  are presented in Table 4.

Moreover, in order to validate the employed numerical method for non-Newtonian nanofluids, the values of convective heat transfer coefficient obtained through the numerical solution was compared with that of [39] for carbon nanotube volume fraction of 1%. The employed geometry in [39] was a pipe of 914.4 mm length with a diameter of 1.55 mm (Table 5). Presented in Table 6, the results of the present study were compared to the numerical results of [39] at two different pipe cross-sections. As shown, the results are in good agreement.

Employing air as the fluid, the obtained numerical solution for a laminar flow within a pipe composed of a porous material and subject to a constant heat flux is compared to the results of [40] in Fig. 3. As shown, a difference of 2.34% is obtained between the two cases.

In the end, in order to fully assure the numerical solution method, the present work is compared with the work of [96]. Fig. 3 Shows the comparison of the present work with the [96] in 1% volume fraction. Their geometry consisted of two 5-m horizontal pipes. They used a combination of water- $Al_2O_3$  nanofluid and porous material under a laminar flow. The nanoparticles diameter used was 38 nm. The results obtained in different Reynolds numbers show good agreement.

## 4. Results and discussion

Fig. 3 demonstrates the dimensionless velocity profile along the pipe cross-section for different values of Darcy number at a thickness ratio of 0.6 and volume fractions of 0% and 1.5%. In the case of non-Newtonian fluids, the apparent viscosity depends on the consistency index and the index of power-law. On the other hand, decreasing the index of power-law results in a more nonlinear relationship between stress and strain rate. This increase in nonlinearity consequently leads to increased viscosity difference in the wall, porous medium and free-flow region. The decreasing shear behavior is further intensified as the index of power law decreases and the volume fraction increases. Presence of the porous layer causes increased velocity gradient. Moreover, in the case of lower permeability values, lower amounts of fluid flow can move from the porous region, i.e. the more resistant region, towards the clean region of lower resistance. This, in turn, leads to increased values of maximum velocities and more non-flat velocity profiles. Additionally, at a given volume fraction and for a fixed porosity, decreases in the permeability leads to increased Darcy velocity and, consequently, velocity profile. For a Darcy number of 0.01, the nanofluid velocity increases by 18.2% as the volume fraction increases from 0% to 1.5%.

Table 2

The grid independency for Nusselt number.

| No. | Number of points along the $\theta$ direction | Number of points along the R direction | Number of points along the Z direction | Number of elements | Nusselt Number | Percentage of variations |
|-----|---|--|--|--------------------|----------------|--------------------------|
| 1   | 20  | 30                                     | 800                                    | 480,000            | 13.6561        | –                        |
| 2   | 25  | 35                                     | 1000                                   | 875,000            | 12.6119        | 7.65                     |
| 3   | 30  | 42                                     | 1100                                   | 1,386,000          | 12.3261        | 2.27                     |
| 4   | 32  | 45                                     | 1200                                   | 1,728,000          | 12.3196        | 0.05                     |

**Table 3**  
Grid independency for dynamic pressure.

| No. | Number of points along the $\theta$ direction | Number of points along the R direction | Number of points along the Z direction | Number of elements | Dynamic pressure (Pa) | Percentage of variations |
|-----|---|--|--|--------------------|-----------------------|--------------------------|
| 1   | 20  | 30                                     | 800                                    | 480,000            | 88.48484              | –                        |
| 2   | 25  | 35                                     | 1000                                   | 875,000            | 89.74097              | 1.42                     |
| 3   | 30  | 42                                     | 1100                                   | 1,386,000          | 89.73443              | 0.007                    |
| 4   | 32  | 45                                     | 1200                                   | 1,728,000          | 89.73221              | 0.002                    |

Fig. 4 demonstrates the dimensionless velocity profile along the radial direction of the pipe for different thickness ratios at a volume fraction of 1.5% and a  $Da = 0.1$ . A flatter velocity profile is observed due to the absence of the porous layer and consequently a higher permeability, which allows for reduced resistance against fluid momentum. At a fixed permeability, a larger portion of the fluid is rejected to the clean region, i.e. the region of lower resistance, as the thickness of the porous layer increases. This, in turn, results in increased velocity profile. Compared to the non-porous case, a 10.27 increase was obtained at the medium thickness of 0.2.

Fig. 5 shows the diagram of pressure drop along the pipe versus different thickness values at different values of Darcy and Reynolds numbers at a volume fraction of 1.5%. The diagram demonstrates an exponential behavior. At a given thickness ratio, the pressure drop increases as the Darcy number is decreased. This can be explained through the increased resistance of the porous layer against the passing fluid as the permeability decreases. The fluid considers this resistance as an obstacle along its flow path. Moreover, at a fixed permeability, the pressure drop is increased as the thickness of the porous layer increases. The pressure drop in the pipe is distributed in two segments. The generated pressure drop by the porous layer is different than that of the clean region, and as the thickness of the porous layer increases, the respective pressure drop in this layer begins to dominate that of the clear region. The effect of these variations is highly evident at a thickness ratio of 0.6. Hence, in addition to improving the heat transfer, employing a porous medium also increases the pressure drop and consequently the required pumping power. The pressure drop in Fig. 5 demonstrates the maximum pressure drop versus volume fractions of 1% and 0%. This increase in the pressure drop in the presence of the porous layer is due to the viscosity and density of the nanofluid. Also, as the thickness of the porous layer increases at fixed values of permeability and porosity, the velocity of the nanofluid is also increased; this consequently maximizes the pressure drop in the pipe for a volume fraction of 1.5%. For Darcy and Reynolds numbers of 0.0001 and 100, respectively, and at a thickness ratio of 0.2, a 50.97% increase is obtained in the presence of a porous layer.

Fig. 6 demonstrates the diagram of pressure drop versus different volume fractions at different Reynolds number in the absence of the porous layer. Increasing volume fraction leads to increased dynamic viscosity and density of the nanofluid. This consequently changes the nanofluid velocity and causes increased generation of momentum as well as pressure drop. This increase in the momentum is more evident in high Reynolds numbers. In case of non-Newtonian fluids, the diagram of pressure drop demonstrates an interesting behavior. As the Reynolds number and volume fraction of the nanofluid increases, the velocity of nanoparticles along the pipe wall is also increased, hence causing an increased shear stress between the fluid and the adjacent wall. For a Reynolds number of 300, a 54.3% increase is observed in the pressure drop at a volume fraction of 1.5% compared to the 0% volume fraction.

**Table 4**  
The effective parameters for the fully developed laminar flow within the circular concentric region subject to constant heat flux at both surfaces [35].

| $Nu_{ii}$ | $Nu_{oo}$ | $\theta_i^*$ | $\theta_o^*$ |
|-----------|-----------|--------------|--------------|
| 5.58      | 5.24      | 0.401        | 0.299        |

The dimensionless temperature profile at the pipe cross-section is illustrated in Fig. 7. As shown, the peak of the temperature profile is increased as the Darcy number increases. Increased permeability leads to a better physical contact between the fluid and the pipe wall, consequently increasing the heat transfer and maximizing the temperature peak. On the other hand, as the permeability is decreased, the porous material intensifies its heat conductivity behavior, ultimately reducing the temperature peak as it causes the temperature of the regions adjacent to the pipe to increase. For a Darcy number of 0.01, a 14.19% increase is obtained in the temperature velocity at the volume fraction of 1.5% compared to that of 0%.

Fig. 8 shows the dimensionless temperature profile along the radial direction for different thickness ratios. At the first glance, the behavior of the diagrams seems to be somehow complex; however, in the absence of the porous layer, the temperature reaches its maximum at the walls, dropping to a minimum as it approaches the center of the pipe. Hence, there exists a high temperature different between the wall and the center of the pipe. By applying the considered thickness ratios to the porous layer, i.e. increasing the thickness of the porous layer, the temperature of the wall as well as the temperature difference between the wall and center of pipe begin to decrease. This decreasing trend with its gentle slope can be seen in the thickness ratio of 0.6. Moreover, an asymmetrically is present at the intersection of the curvatures as the temperatures of the upper and lower pipes are not equal. An increase of 86.74% is obtained in the temperature profile at the thickness ratio of 0.6 compared to the case where no porous medium is present.

Figs. 9 to 14 demonstrate the value of local convective heat transfer coefficient along the pipe for different volume fractions and Reynolds numbers. This coefficient generally demonstrates a decreasing behavior along the pipe axis. For a constant heat flux and as the fluid enters the pipe, the temperature gradient is considerably large at the beginning of the pipe, since the thermal boundary layer has not grown yet. As the fluid proceeds further and the thermal boundary layer grows, the temperature difference between the channel wall and the bulk temperature of the fluid is increased. The rate of this decrease is gradually decreased along the pipe, ultimately reaching a constant value under fully developed conditions. It should be noted that due to the rheological properties of power-law non-Newtonian fluids, the length of the thermally developed region is considerably long. Unlike Newtonian fluids, such fluids assume considerably high Prandtl numbers. Additionally, the values of the convective heat transfer coefficient are increased as the volume fraction increases. In fact, at a fixed Reynolds number, increasing the viscosity is accompanied by an increase the concentration of the nanofluid in the denominator of the Reynolds number. Hence, increasing the volume fraction leads to increased thermal conductivity,

**Table 5**  
Comparison of the obtained results in the present study with [35].

| $Nu_i$            |               | $Nu_o$            |               |
|-------------------|---------------|-------------------|---------------|
| Ref. [35]         | Current study | Ref. [35]         | Current study |
| 9.35              | 9.21          | 7.48              | 7.46          |
| Percent error (%) |               | Percent error (%) |               |
| 1.5               |               | 0.27              |               |

**Table 6**  
Comparison of the present study with [39].

| $\frac{x}{D}$ | Reference [39] $h$ (W/m <sup>2</sup> K) | Current study $h$ (W/m <sup>2</sup> K) | Percent error (%) |
|---------------|---|--|-------------------|
| 80            | 2276.7                                  | 2399.33                                | 5.38              |
| 100           | 2190.71                                 | 2273.17                                | 3.76              |

which, in turn, increases the convective heat transfer coefficient. Moreover, the convective heat transfer coefficient is also increased by increasing the Reynolds number. Since the Reynolds number is representative of the ratio of inertia to viscous forces, at a fixed volume fraction of nanoparticles and hence fixed viscous forces, increasing or decreasing the Reynolds number leads to increased or decreased inertia forces, respectively. Moreover, as the Darcy number increases, the convective heat transfer coefficient is also increased. In case of applying a layer of the porous material to the walls, the value of convective heat transfer coefficient as well as the thickness of the thermal boundary layer are increased, the reason for which may be attributed to the increased conductive heat transfer from the channel wall towards the porous region, which ultimately increases the heat transfer. Considering that the Darcy number is representative of permeability, increasing its value enhances the fluid penetrability within the porous medium, and hence the fluid can more easily move towards the pipe wall from the porous region. On the other hand, given that the walls are subject to constant heat fluxes, as the permeability increases, the temperature difference is decreased between the pipe wall and bulk temperature along the pipe, consequently leading to increased values of convective heat transfer coefficient. For a  $Re = 100$ , a 12.97% increase is achieved in the local convective heat transfer coefficient at the volume fraction of 0% compared to the case where no porous layer is present.

Figs. 15 and 16 demonstrate diagrams of local convective heat transfer coefficient along the pipe axis for given values of the Darcy number and volume fraction at different values of Reynolds numbers and thickness of the porous layer. As shown, in the case where the thickness of the porous layer increases, the variation domain of convective heat transfer coefficient is broader than that of the case where the values of the Darcy number vary at a given thickness. Moreover, the porous region reduces the temperature difference between the pipe wall and the mean temperature of the fluid. In addition, the effect of the porous layer on increasing the convective heat transfer coefficient is larger than the Reynolds number, since, at a given volume fraction, the porous medium plays a greater role in increasing the heat transfer compared to

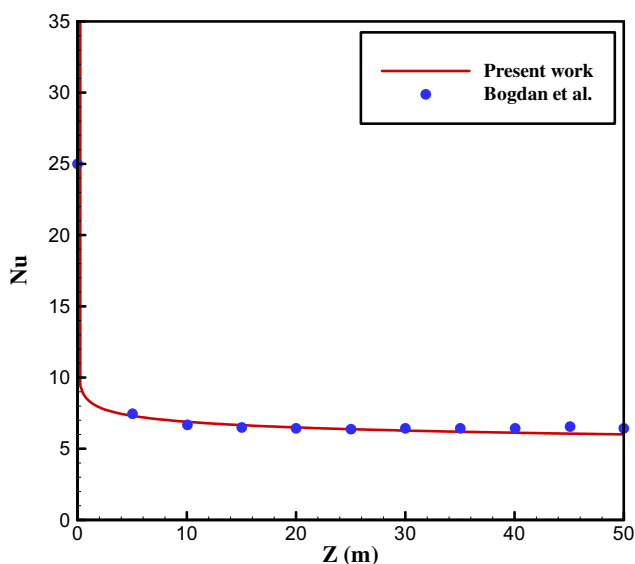


**Fig. 3.** Comparison of the present study with [40].

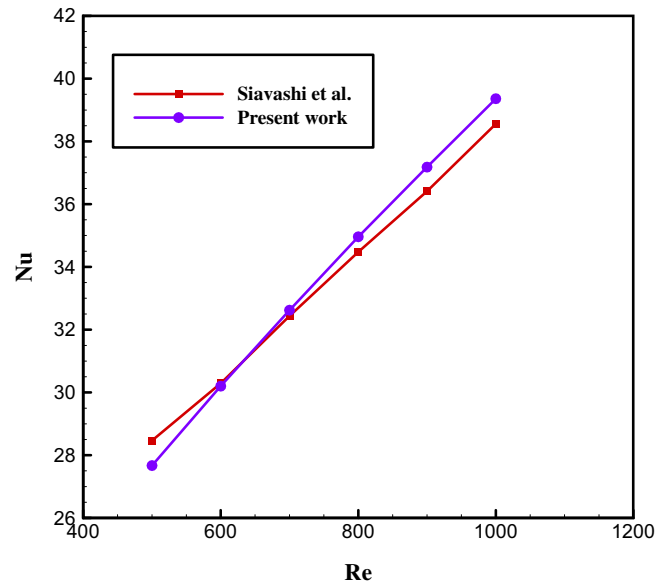


**Fig. 4.** Comparison of the present study with [96].

the increasing Reynolds number. The porous medium achieves this by increasing the contact surface with the metal foam as a way to increase the heat transfer.

Figs. 17 and 18 demonstrate diagrams of the Nusselt number versus the thickness of the porous medium for the outer and inner pipes, respectively. The Nusselt number assumes the maximum values for  $R_p = 0.6$ , the reason for which can be associated with the arrangement of the porous material, its thermal conductivity, and the fact that a large portion of the pipe is filled with the porous material. Since the porous material further increases the velocity gradient and ultimately the mean velocity remains constant at a certain permeability, the heat transfer is increased overall. In case no porous layers are present, the maximum Nusselt number occurs at a volume fraction of 1.5%, which can be due to the increased thermal conductivity in nanofluids. Another reason can be associated with the increased fluid velocity according to Eq. 6.6, which is caused by the increase in the consistency index. Since the porous material is located on the walls, lower values of permeability

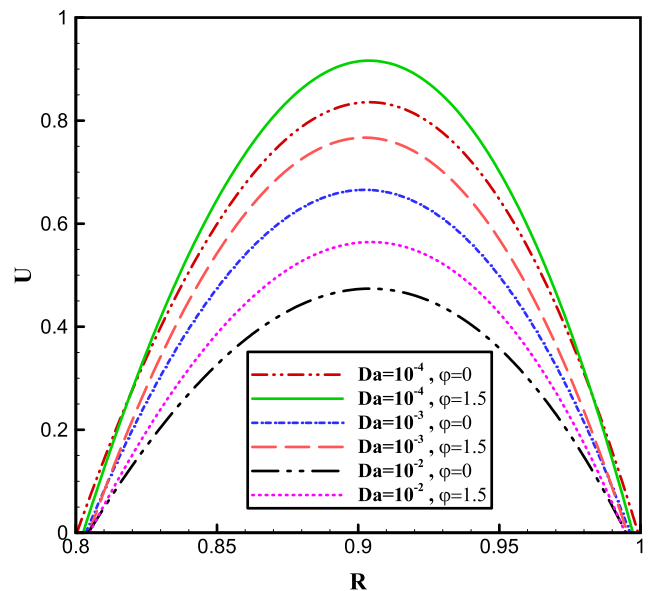


**Fig. 5.** Dimensionless velocity profile along the radial direction for different Darcy numbers as well as different volume fractions at a thickness ratio of 0.6.

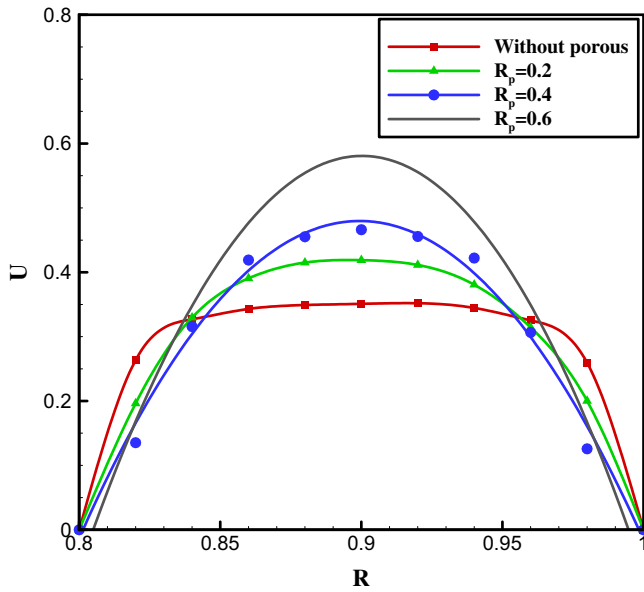


Fig. 6. Dimensionless velocity profile along the radial direction at a volume fraction of 1.5% and a  $Da = 0.01$ .

cause smaller portions of the fluid to move towards the free region, due to which a thinner boundary layer is formed and the heat transfer is decreased at a given thickness. The Nusselt number increases as the thickness of the porous medium is increased. As shown, the value of Nusselt number for the outer pipe is smaller than that of the inner, which is due to the higher temperature of the latter than that of the former. In fact, in case of similar fluxes applied to both surfaces, a lower heating value is ultimately absorbed by the surface of the inner wall as its area is lower than that of the outer wall (the bulk temperature of both pipes are similar). On the other hand, as the thickness of the porous layer increases, the occupied share of the clean region is gradually decreased and hence the Nusselt number is abruptly increased. For a Darcy number of 0.0001 and at a volume fraction of 1.5%, a 23.78% increase is achieved in the Nusselt number for the thickness ratio of 0.2 compared to the case where no porous layers are present.

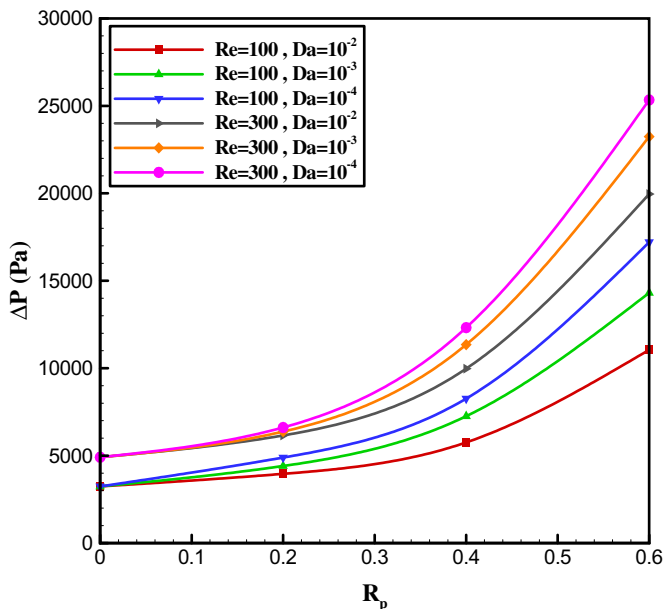


Fig. 7. Pressure drop versus different porous thickness ratios for different values of Darcy and Reynolds numbers at a volume fraction of 1.5%.

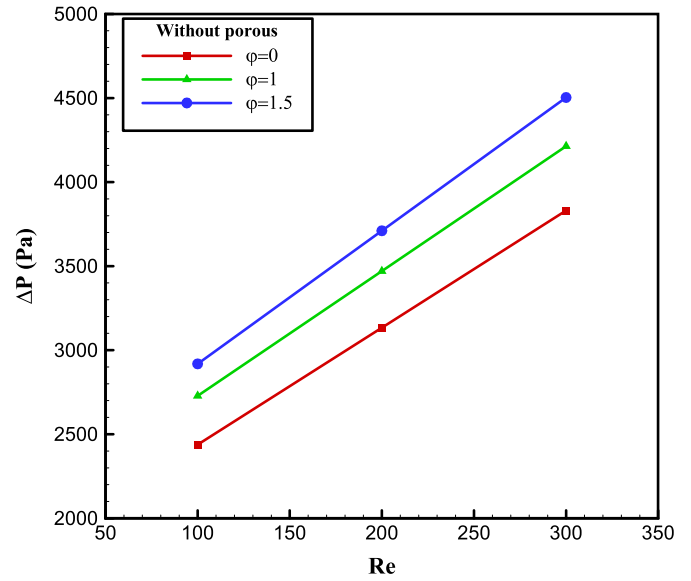


Fig. 8. Pressure drop versus the Reynolds number for different volume fractions.

Incorporating porous media to enhance heat transfer of heat exchangers leads to significant increase in the pressure drop and the pumping power. Hence, a compromise between these two factors is to be achieved so that the employed method for performance improvement can be evaluated more effectively. The variable employed in this regard is defined as the performance evaluation criterion (PEC) and is expressed through the following eq. [95],

$$PEC = \frac{Nu / Nu_s}{\left(\frac{f}{f_s}\right)^{1/3}} \quad (35)$$

where  $Nu$  and  $f$ , respectively, represent the Nusselt number and coefficient of pressure drop in the presence of a porous medium, and  $Nu_s$  and  $f_s$  indicate the same parameters for a simple channel.

Fig. 19 demonstrates the diagram of PEC for a thickness ratio of 0.2. As the volume fraction increases, the PEC increases due to the increased

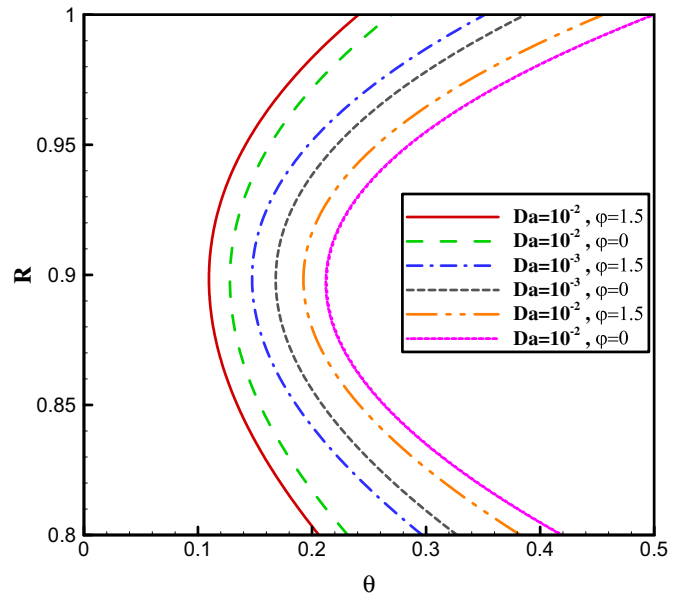


Fig. 9. Dimensionless temperature profile along the radial direction of the pipe for different volume fractions as well as Darcy numbers at a thickness ratio of 0.6.

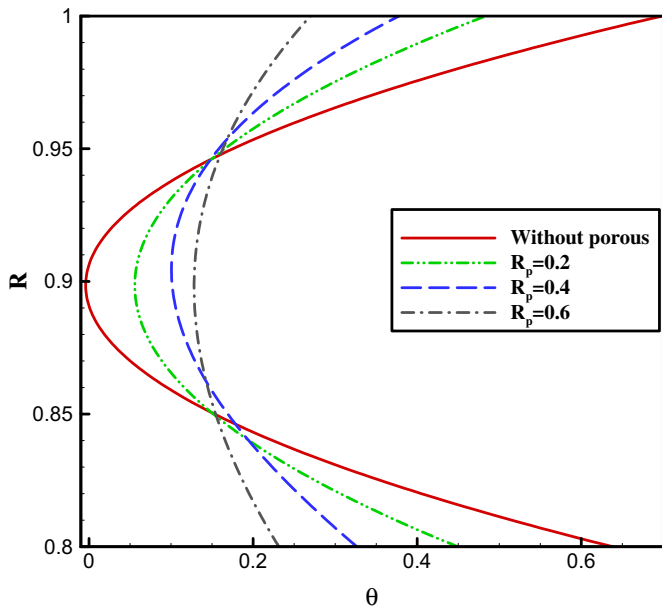


Fig. 10. Dimensionless temperature profile along the radial direction for different thickness ratios at a  $Da = 0.01$ .

shear rate on the pipe walls. Generally, in case  $PEC < 1$ , the dissipated energy through pressure drop is less than that caused by the porous medium, which is an indication of a favorable efficiency. Hence, the  $PEC$  in this case is higher than the case where no porous medium is present in the pipe. In the mentioned form, we see a decreasing and increasing behavior, the reason for this behavior can be due to the permeability property of porous material with the non-Newtonian nanofluid. This behavior is obvious in the science of heat transfer, because in some studies researchers, in the field of heat transfer also seen mixed convection, which is within a certain range of Grashof number that may decrease or increase heat transfer and thermal performance [97]. Also, it should be noted that the economic efficiency should also be taken into consideration. The best case occurs by assuming a  $Da = 0.01$ , for which and at a volume fraction of 1.5%, the  $PEC$  increases by 7.29% compared to the

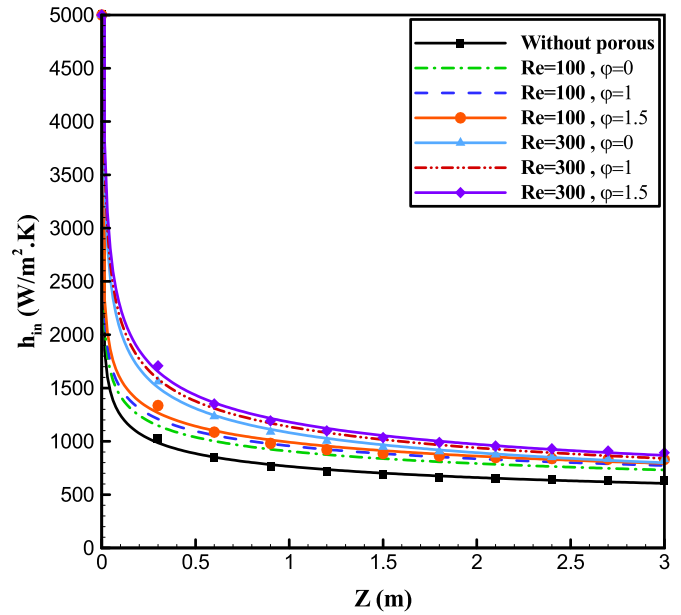


Fig. 12. Local convective heat transfer coefficient along the axis of the inner pipe at Darcy number and thickness ratio of 0.0001 and 0.2, respectively.

Darcy number and volume fraction of 0.0001 and 1.5, percent, respectively.

Fig. 20 demonstrates the diagram of  $PEC$  versus the thickness of the porous layer at different volume fractions of the nanofluid. The qualitative descriptions are similar to of Fig. 19, with the exception of the  $PEC$  varying in a broader range compared to the case where the Darcy number varies at a given thickness. Since the best performance is associated with a thickness ratio of 0.6, use of the nanofluid at any given volume fraction of the base fluid does not significantly improve the performance. For a thickness ratio of 0.4 and at a volume fraction of 1.5%, an increase of 38.6% was achieved compared to the thickness ratio of 0.2.

Two different thermal models can be used in the energy equation, namely the local thermal equilibrium model and the local thermal non-equilibrium model. The former assumes that at each point, the

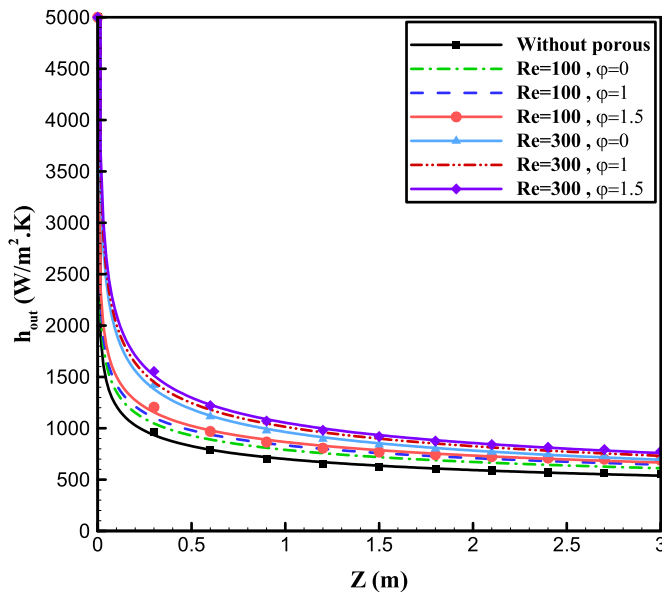


Fig. 11. Local convective heat transfer coefficient along the axis of the outer pipe at Darcy number and thickness ratio of 0.0001 and 0.2, respectively.

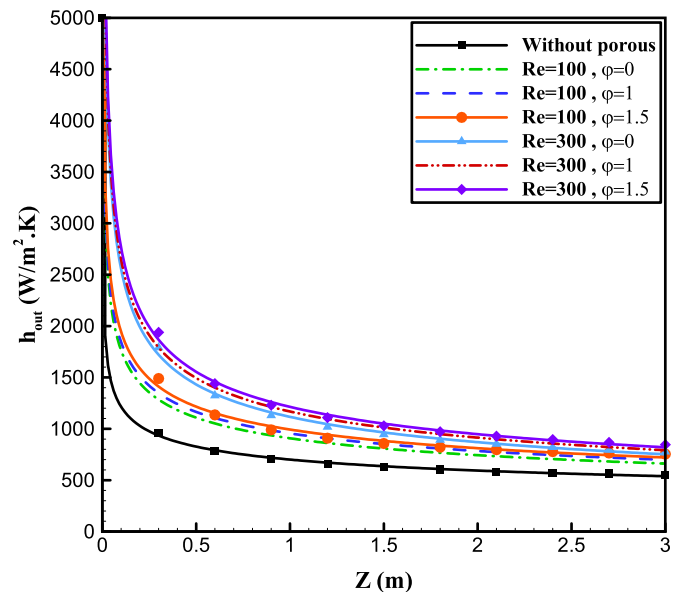


Fig. 13. Local convective heat transfer coefficient along the axis of the outer pipe at Darcy number and thickness ratio of 0.001 and 0.2, respectively.

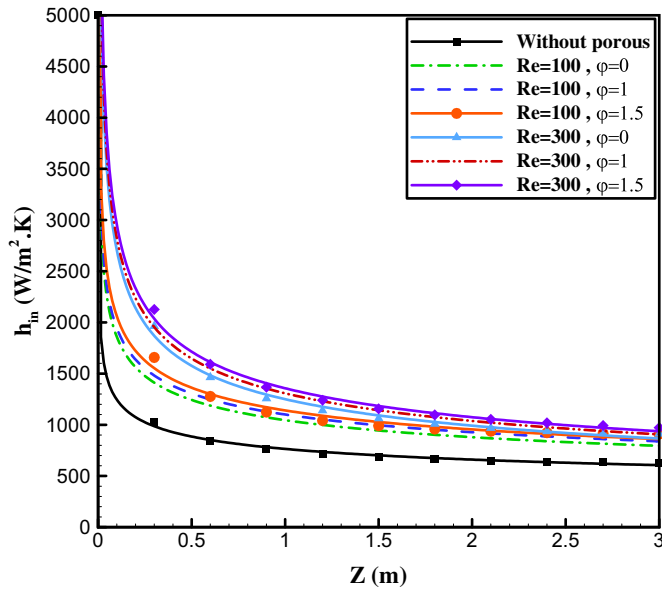


Fig. 14. Local convective heat transfer coefficient along the axis of the inner pipe at Darcy number and thickness ratio of 0.001 and 0.2, respectively.

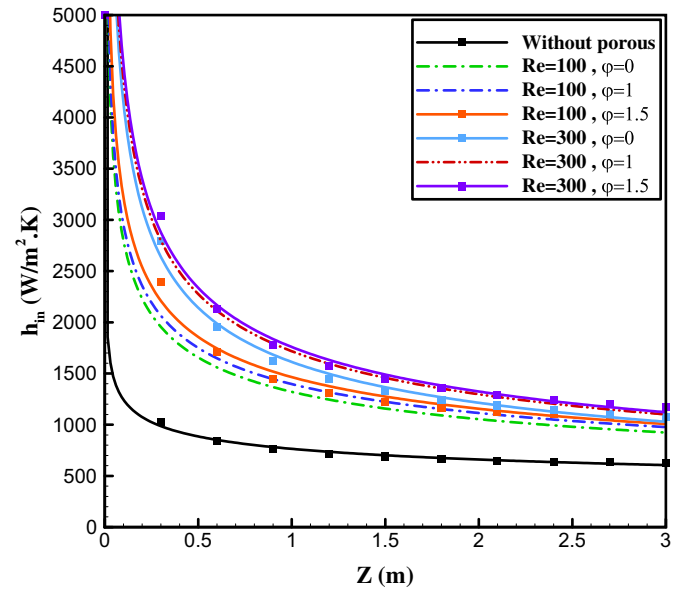


Fig. 16. Local convective heat transfer coefficient along the axis of the inner pipe at Darcy number and thickness ratio of 0.01 and 0.2, respectively.

temperature of the solid phase in the porous medium is roughly equal to the temperature of the fluid, meaning that the liquid and solid phases are in thermal equilibrium at each point of the medium. This assumption is theoretically and numerically simple. Merely one energy equation is solved in this model. In fact, in this model  $T_s = T_f = T$ , where  $T_s$  and  $T_f$  are, respectively, the solid and fluid temperatures at each point. Generally, no rules are available to determine the allowed ranges of the parameters in the thermal equilibrium model, and the literature studies have investigated different arrangements of the porous medium by considering different geometries and values of thermal conductivity.

Fig. 21 demonstrates the diagram of Nusselt number along the pipe axis for Darcy number and thickness ratio of 0.0001 and 0.2, respectively. Let us define the parameter  $Kr$  as the ratio of the effective thermal conductivity of the fluid and the porous environment to the fluid

thermal conductivity. By assuming  $Kr = 1$ , the value of Nusselt number is lower than that of the case where no porous layer is present. In such a case, the porous medium acts as a thermal insulation and causes the heat transfer to decrease. This is not economically beneficial, since in addition to a decreased heat transfer; the pressure drop caused by the porous material is increased compared to the case where the porous material is not present. Hence, use of a porous medium to increase heat transfer is only justifiable in case a considerable improvement is achieved in the heat transfer compared to the case where no porous medium is present. According to the figure, the value of  $Kr$  should be higher than 5 to obtain a significant increase in the heat transfer compared to the case with no porous material. An increase of 1.91% is achieved in the Nusselt number for  $Kr = 5$  compared to the case where no porous material is present (Figs. 22–23).

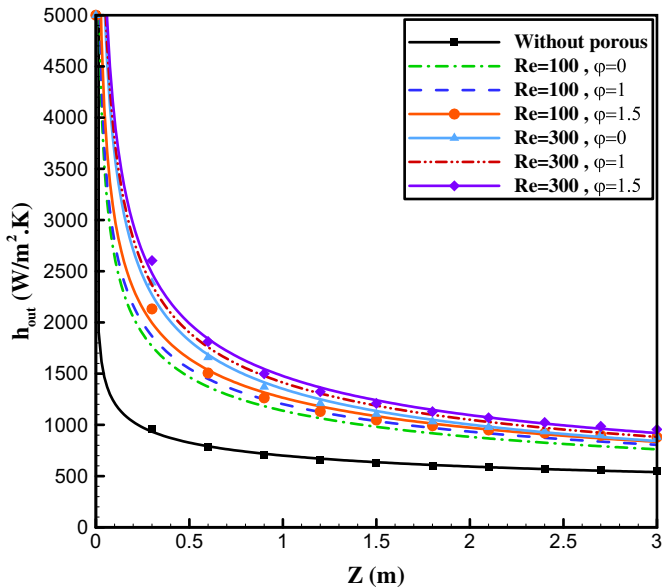


Fig. 15. Local convective heat transfer coefficient along the axis of the outer pipe at Darcy number and thickness ratio of 0.01 and 0.2, respectively.

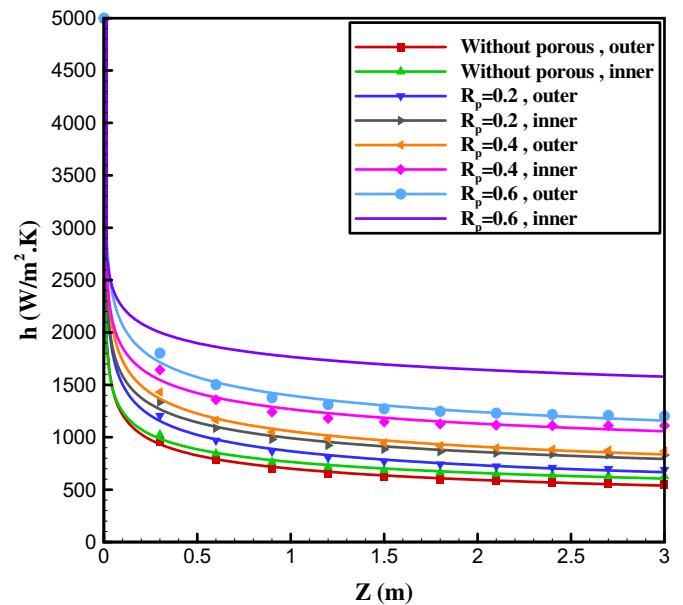


Fig. 17. Local convective heat transfer coefficient along the pipe axis for different thickness ratios at volume fraction and Reynolds and Darcy numbers of 1.5%, 100, and 0.0001, respectively.

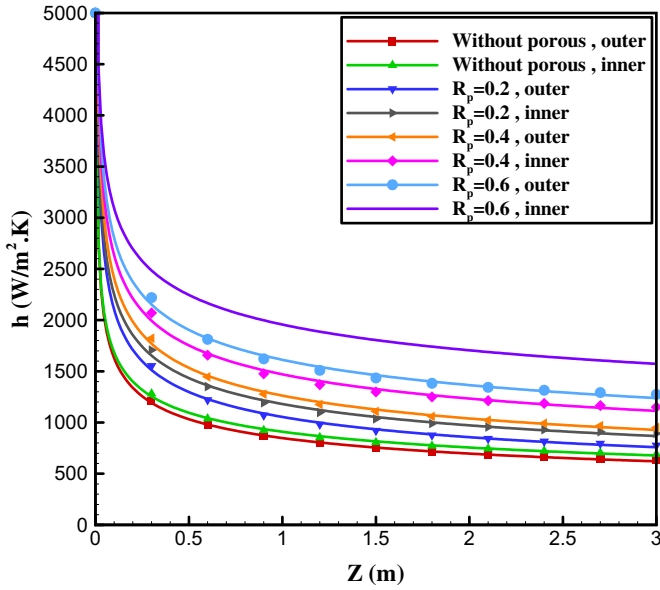


Fig. 18. Local convective heat transfer coefficient along the pipe axis for different thickness ratios at volume fraction and Reynolds and Darcy numbers of 1.5%, 300, and 0.0001, respectively.

5. Conclusion

In this paper, the comprehensive study of laminar flow and heat transfer of pseudo-plastic non-Newtonian nanofluid ( $Al_2O_3 + CMC$ ) within the porous circular concentric is investigated. Simulations for different Reynolds numbers and Darcy numbers in the range of  $100 \leq Re \leq 300$  and  $10^{-4} \leq Da \leq 10^{-2}$  are done. The following results can be deduced from our simulation:

- At a fixed permeability, a larger portion of the fluid is rejected to the clean region, i.e. the region of lower resistance, as the thickness of the porous layer increases

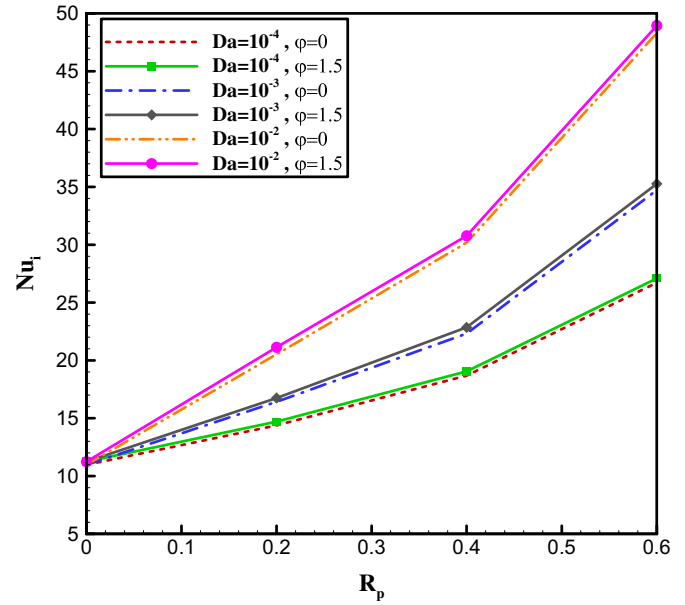


Fig. 20. Average Nusselt number versus porous thickness ratios for different values of Darcy and Reynolds numbers at a volume fraction of 1.5% for inner pipe.

- At a given volume fraction and for a fixed porosity, decreases in the permeability leads to increased Darcy velocity and, consequently, velocity profile. As the thickness of the porous layer increases at fixed values of permeability and porosity, the velocity of the nanofluid is also increased;
- As the thickness of the porous layer increases, the occupied share of the clean region is gradually decreased and hence the Nusselt number is abruptly increased.
- At a given volume fraction, the porous medium plays a greater role in increasing the heat transfer compared to the increasing Reynolds number.
- An increase of 1.91% is achieved in the Nusselt number for  $Kr = 5$  compared to the case where no porous material is present.

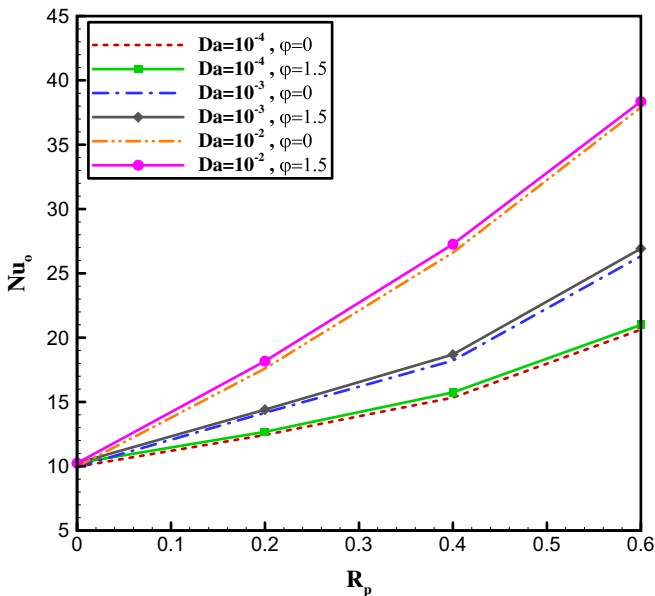


Fig. 19. Average Nusselt number versus porous thickness ratios for different values of Darcy and Reynolds numbers at a volume fraction of 1.5% for outer pipe.

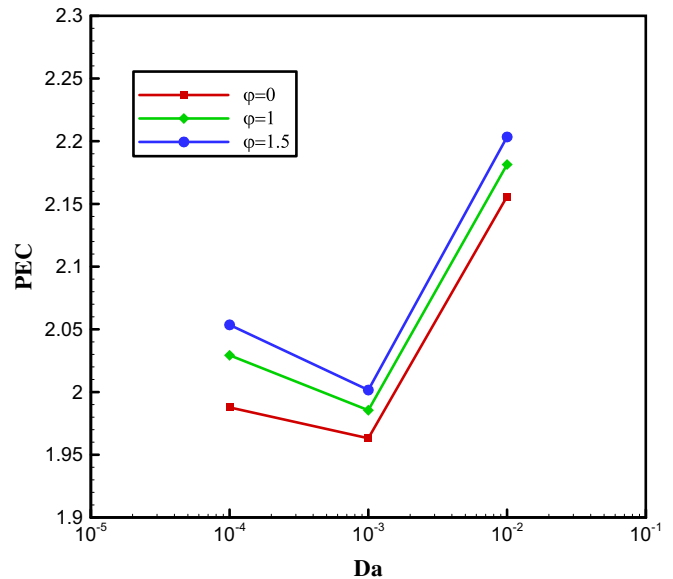


Fig. 21. Diagram of PEC versus the Darcy number at different volume fractions for a thickness ratio of 0.2.

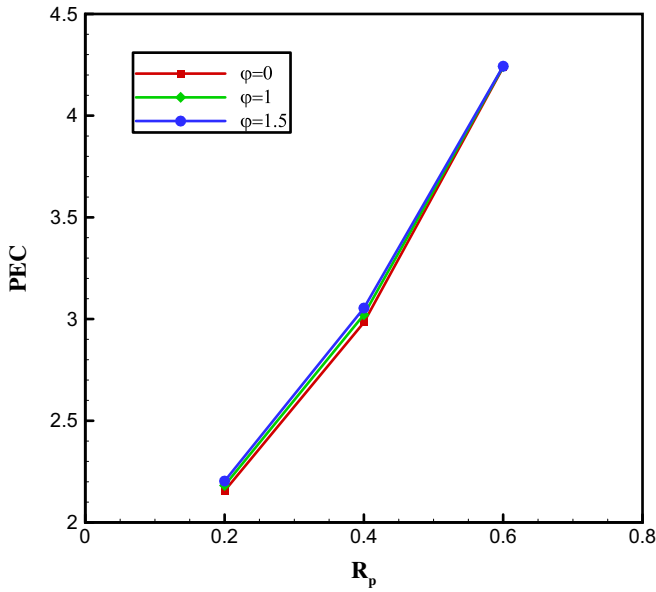


Fig. 22. Diagram of PEC versus the thickness ratio of the porous layer at different volume fractions of the nanofuid for a  $Da = 0.01$ .

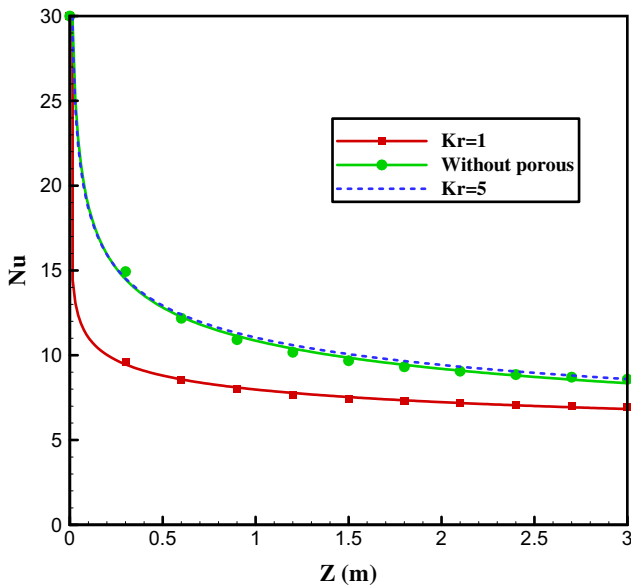


Fig. 23. Nusselt number along the pipe axis for a volume fraction of 1.5% and different values of thermal conductivity at the Darcy number and thickness ratio of 0.0001 and 0.2, respectively.

The extension of this paper for nanofuid according our previous works [41–93] affords engineers a good option for micro and nano simulation.

References

[1] Thomas G. Mezger, *The Rheology Handbook: For Users of Rotational and Oscillatory Rheometers*, 2., rev. ed. Vincentz Network, Hannover, 2006 34 (ISBN 9783878701743).  
 [2] R. Paul Singh Heldman, R. Dennis, *Introduction to Food Engineering*, 5th ed Elsevier, Amsterdam, 2013 160.  
 [3] Xianfeng Zheng, Guofang Shen, Chao Wang, Yu Li, Darren Dunphy, Tawfiq Hasan, C. Jeffrey Brinker, Bao-Lian Su, *Bio-inspired Murray Materials for Mass Transfer and Activity*, 2017 (Nature Communications).

[4] S.U.S. Choi, *Enhancing Thermal Conductivity of Fluids with Nanoparticles*, 66, American Society of Mechanical Engineers—Fluids Engineering Division Publication, New York, 1995 99–105.  
 [5] J.A. Eastman, S.U.S. Choi, S. Li, W. Yu, L.J. Thompson, Anomalous increased effective thermal conductivities of ethylene glycol-based nanofluids containing copper nanoparticles, *Appl. Phys. Lett.* 78 (2001) 718–720.  
 [6] H.A. Mintsa, G. Roy, C.T. Nguyen, D. Doucet, New temperature dependent thermal conductivity data for water-based nanofluids, *Int. J. Therm. Sci.* 48 (2009) 363–371.  
 [7] Mohsen Sheikholeslami, Magnetohydrodynamic nanofluid forced convection in a porous lid driven cubic cavity using lattice Boltzmann method, *Journal of Molecular Liquids Volume 231* (April 2017) 555–565.  
 [8] M. Sheikholeslami, M.M. Rashidi, D.D. Ganji, Effect of non-uniform magnetic field on forced convection heat transfer of  $Fe_3O_4$ -water nanofluid, *Computer Methods in Applied Mechanics and Engineering* 294 (1) (September 2015) 299–312.  
 [9] M. Sheikholeslami, D.D. Ganji, M.M. Rashidi, Magnetic field effect on unsteady nanofluid flow and heat transfer using Buongiorno model, *J. Magn. Magn. Mater.* 416 (15) (2016) 164–173.  
 [10] M. Sheikholeslami, D.D. Ganji, Nanofluid convective heat transfer using semi analytical and numerical approaches: a review, *J. Taiwan Inst. Chem. Eng.* 65 (August 2016) 43–77.  
 [11] M. Sheikholeslami, D.D. Ganji, Nanofluid hydrothermal behavior in existence of Lorentz forces considering Joule heating effect, *J. Mol. Liq.* 224 (Part A) (December 2016) 526–537.  
 [12] M. Sheikholeslami, Influence of magnetic field on nanofluid free convection in an open porous cavity by means of lattice Boltzmann method, *Journal of Molecular Liquids Volume 234* (May 2017) 364–374.  
 [13] Ching-Yang Cheng, Free convection of non-Newtonian nanofluids about a vertical truncated cone in a porous medium, *Int. Commun. Heat Mass Transf.* 39 (2012) 1348–1353.  
 [14] M. Hatami, D.D. Ganji, Heat transfer and flow analysis for SA-TiO<sub>2</sub> non-Newtonian nanofluid passing through the porous media between two coaxial cylinders, *J. Mol. Liq.* 188 (2013) 155–161.  
 [15] D.A. Nield, A.V. Kuznetsov, Forced convection in a parallel-plate channel occupied by a nanofluid or a porous medium saturated by a nanofluid, *Int. J. Heat Mass Transf.* 70 (2014) 430–433.  
 [16] S.J. Uphill, Terence Cosgrove, Wuge H. Briscoeb, Flow of nanofluids through porous media: preserving timber with colloid science, *Colloids Surf. A Physicochem. Eng. Asp.* 460 (2014) 38–50.  
 [17] G.C. Bourantas, E.D. Skouras, V.C. Loukopoulou, V.N. Burganos, Heat transfer and natural convection of nanofluids in porous media, *Eur. J. Mech. B. Fluids* 43 (2014) 45–56.  
 [18] M.A. Sheremet, I. Pop, Free convection in a triangular cavity filled with a porous medium saturated by a nanofluid: Buongiorno’s mathematical model, *Int. J. Numer. Methods Heat Fluid Flow* 25 (2015) 1138–1161.  
 [19] Raed AbedMahdi, H.A. Mohammed, K.M. Munisamy, N.H. Saeid, Review of convection heat transfer and fluid flow in porous media with nanofluid, *Renew. Sust. Energ. Rev.* 41 (2015) 715–734.  
 [20] G.H.R. Kefayati, Heat transfer and entropy generation of natural convection on non-Newtonian nanofluids in a porous cavity, *Powder Technol.* 299 (2016) 127–149.  
 [21] S. Sivasankaran, K. Narrein, Numerical investigation of two-phase laminar pulsating nanofluid flow in helical microchannel filled with a porous medium, *Int. Commun. Heat Mass Transf.* 75 (2016) 86–91.  
 [22] M. Ghalambaz, M. Sabour, I. Pop, Free convection in a square cavity filled by a porous medium saturated by a nanofluid: viscous dissipation and radiation effects, *Engineering Science and Technology, an International Journal* 19 (2016) 1244–1253.  
 [23] M. Devakar, K. Ramesh, Sagar Chouhan, Ankush Raje, Fully developed flow of non-Newtonian fluids in a straight uniform square duct through porous medium, *Journal of the Association of Arab Universities for Basic and Applied Sciences* (2016), <https://doi.org/10.1016/j.jaubas.2016.04.001>.  
 [24] Alibakhsh Kasaean, Reza Daneshazarian, Omid Mahian, Lioua Kolsi, Ali J. Chamkha, Somchai Wongwises, Ioan Pop, Nanofluid flow and heat transfer in porous media: a review of the latest developments, *Int. J. Heat Mass Transf.* 107 (2017) 778–791.  
 [25] Fatih Selimefendigil, Muneer A. Ismael, Ali J. Chamkha, Mixed convection in superposed nanofluid and porous layers in square enclosure with inner rotating cylinder, *Int. J. Mech. Sci.* 124–125 (2017) 95–108.  
 [26] A. Brusly Solomon, M. Sharifpur, Tanja Ottermann, Carla Grobler, Michael Joubert, Josua P. Meyer, Natural convection enhancement in a porous cavity with Al<sub>2</sub>O<sub>3</sub>-ethylene glycol/water nanofluids, *Int. J. Heat Mass Transf.* 108 (2017) 1324–1334.  
 [27] P. Sudarsana Reddy, P. Sreedevi, Ali J. Chamkha, Boundary layer flow, heat and mass transfer analysis over a rotating disk through porous medium saturated by Cu-water and Ag-water nanofluid with chemical reaction, *Powder Technol.* 307 (2017) 46–55.  
 [28] Heidar Hashemi, Zafar Namazian, S.A.M. Mehryan, Cu-water micropolar nanofluid natural convection within a porous enclosure with heat generation, *J. Mol. Liq.* 236 (2017) 48–60.  
 [29] Abdelraheem M. Aly, Natural convection over circular cylinders in a porous enclosure filled with a nanofluid under thermo-diffusion effects, *J. Taiwan Inst. Chem. Eng.* 70 (2017) 88–103.  
 [30] B.C. Pak, Y.I. Cho, Hydrodynamic and heat transfer study of dispersed fluids with submicron metallic oxide particles, *Experimental Heat Transfer an International Journal* 11 (2) (1998) 141–170.  
 [31] Y. Xuan, W. Roetzel, Conceptions for heat transfer correlation of nanofluids, *Int. J. Heat Mass Transf.* 43 (19) (2000) 3701–3707.  
 [32] C.H. Chon, K.D. Kihm, S.P. Lee, S.U.S. Choi, Empirical correlation finding the role of temperature and particle size for nanofluid, thermal conductivity enhancement, *Appl. Phys. Lett.* 87 (15) (2005).

- [33] M. Hojjat, S.Gh. Etemad, R. Bagheri, J. Thibault, Rheological characteristics of non-newtonian nanofluids: experimental investigation, *Int. Commun. Heat Mass Transfer* 38 (2011) 144–148.
- [34] A.V. Shenoy, Non-Newtonian Fluid Heat Transfer in Porous Media, 24, Department of Energy of Mechanical Engineering, Shizuoko University, Japan, 1994.
- [35] F.P. Incropera, D. Dewitt, S.L. Adrienne, Fundamentals of Heat and Mass Transfer, 7th Edition Wiley, 2014.
- [36] J.P. Meyer, T.J. McKrell, K. Grote, The influence of multi-walled carbon nanotubes on single-phase heat transfer and pressure drop characteristics in the transitional flow regime of smooth tubes, *Int. J. Heat Mass Transf.* 58 (2013) 597–609.
- [37] S. Ergun, Fluid flow through packed columns, *Chem. Eng. Prog.* 48 (2) (1952) 89–94.
- [38] B. Farajollahi, S.G. Etemad, M. Hojjat, Heat transfer of nanofluids in a shell and tube heat exchanger, *Int. J. Heat Mass Transf.* 53 (1) (2010) 12–17.
- [39] R. Kamali, A.R. Binesh, Numerical investigation of heat transfer enhancement using carbon nanotube base non-Newtonian nanofluids, *Int. Commun. Heat Mass Transfer* 37 (2010) 1153–1157.
- [40] I.P. Bogdan, A.M. Abdulmajeed, An experimental and numerical study on heat transfer enhancement for gas heat exchangers fitted with porous media, *Int. J. Heat Mass Transf.* 47 (2004) 4939–4952.
- [41] L. Huang, M.S. El-Genk, J.M. Tourmier, Transient performance of an inclined Water heat pipe with a screen wick, *SME National Heat Transfer Conf, Atlanta GA Heat Pipes and Capillary Pumped Loops HTD*, 24, 1993, pp. 87–92.
- [42] M. Hemmat Esfe, M.R. Hassani Ahangar, M. Rejvani, D. Toghraie, M.H. Hajmohammad, Designing an artificial neural network to predict dynamic viscosity of aqueous nanofluid of TiO<sub>2</sub> using experimental data, *Int. Commun. Heat Mass Transfer* 75 (2016) 192–196.
- [43] M. Afrand, D. Toghraie, N. Sina, Experimental study on thermal conductivity of water-based Fe<sub>3</sub>O<sub>4</sub> nanofluid: development of a new correlation and modeled by artificial neural network, *Int. Commun. Heat Mass Transfer* 75 (2016) 262–269.
- [44] M. Afrand, D. Toghraie, N. Sina, Experimental study on thermal conductivity of water-based Fe<sub>3</sub>O<sub>4</sub> nanofluid: development of a new correlation and modeled by artificial neural network, *Int. Commun. Heat Mass Transfer* 75 (2016) 262–269.
- [45] M. Afrand, N. Sina, H. Teimouri, A. Mazaheri, M.R. Safaei, M. Hemmat Esfe, J. Kamali, D. Toghraie, Effect of magnetic field on free convection in inclined cylindrical annulus containing molten potassium, *Int. J. Appl. Mech.* 7 (04) (2015) 1550052.
- [46] H. Noorian, D. Toghraie, A.R. Azimian, Molecular dynamics simulation of Poiseuille flow in a rough nano channel with checker surface roughnesses geometry, *Heat Mass Transf.* 50 (1) (2014) 105–113.
- [47] M. Zarringhalam, A. Karimipour, D. Toghraie, Experimental study of the effect of solid volume fraction and Reynolds number on heat transfer coefficient and pressure drop of CuO–water nanofluid, *Exp. Thermal Fluid Sci.* 76 (2016) 342–351.
- [48] D. Toghraie, A.R. Azimian, Molecular dynamics simulation of liquid–vapor interface on the solid surface using the GEAR'S algorithm, *Dynamics* 182 (2009) 15493.
- [49] D.T. Semiromi, A.R. Azimian, Molecular dynamics simulation of non-droplets with the modified Lennard-Jones potential function, *Heat Mass Transf.* 47 (2010) 579–588.
- [50] D.T. Semiromi, A.R. Azimian, Nanoscale Poiseuille flow and effects of modified Lennard–Jones potential function, *Heat Mass Transf.* 46 (2010) 791–801.
- [51] D.T. Semiromi, A.R. Azimian, Molecular dynamics simulation of liquid–vapor phase equilibrium by using the modified Lennard–Jones potential function, *Heat Mass Transf.* 46 (2010) 287–294.
- [52] S.A. Sajadifar, A. Karimipour, D. Toghraie, Fluid flow and heat transfer of non-Newtonian nanofluid in a microtube considering slip velocity and temperature jump boundary conditions, *Eur. J. Mech. B. Fluids* 61 (2017) 25–32.
- [53] M. Rezaei, A.R. Azimian, D.T. Semiromi, The surface charge density effect on the electro-osmotic flow in a nanochannel: a molecular dynamics study, *Heat Mass Transf.* 51 (2015) 661–670.
- [54] M. Rezaei, A.R. Azimian, D. Toghraie, Molecular dynamics study of an electro-kinetic fluid transport in a charged nanochannel based on the role of the stern layer, *Physica A* 426 (2015) 25–34.
- [54] Mohsen Sheikholeslami, Davood Domiri Ganji, Numerical investigation of nanofluid transportation in a curved cavity in existence of magnetic source, *Chem. Phys. Lett.* 667 (January 2017) 307–316.
- [55] M. Sheikholeslami, D.D. Ganji, Transportation of MHD nanofluid free convection in a porous semi annulus using numerical approach, *Chem. Phys. Lett.* 669 (February 2017) 202–210.
- [56] M. Sheikholeslami, D.D. Ganji, Free convection of Fe<sub>3</sub>O<sub>4</sub>-water nanofluid under the influence of an external magnetic source, *J. Mol. Liq.* 229 (March 2017) 530–540.
- [57] S. Nazari, D. Toghraie, Numerical simulation of heat transfer and fluid flow of water-CuO nanofluid in a sinusoidal channel with a porous medium, *Physica E: Low-dimensional Systems and Nanostructures* 87 (2017) 134–140.
- [58] M.R. Faridzadeh, D.T. Semiromi, A. Niroomand, Analysis of laminar mixed convection in an inclined square lid-driven cavity with a nanofluid by using an artificial neural network, *Heat Transfer Research* 45 (2014).
- [59] M.A. Eshfahani, D. Toghraie, Experimental investigation for developing a new model for the thermal conductivity of silica/water–ethylene glycol (40%–60%) nanofluid at different temperatures and solid volume fractions, *J. Mol. Liq.* 232 (2017) 105–112.
- [60] A. Aghanajafi, D. Toghraie, B. Mehmandoust, Numerical simulation of laminar forced convection of water–CuO nanofluid inside a triangular duct, *Physica E: Low-dimensional Systems and Nanostructures* 85 (2017) 103–108.
- [61] M. Zadkhan, D. Toghraie, A. Karimipour, Developing a new correlation to estimate the thermal conductivity of MWCNT–CuO/water hybrid nanofluid via an experimental investigation, *J. Therm. Anal. Calorim.* (2017), <https://doi.org/10.1007/s10973-017-6213-8>.
- [62] D. Toghraie Semiromi, A.R. Azimian, Molecular dynamics simulation of slab geometry and the effect of cut-off radius, *Proceeding of the 13th Asian Congress of Fluid Mechanics*, 2010.
- [63] S. Shareghi, D. Toghraie, Numerical simulation of blood flow in healthy arteries by use of the Sisko model, *Computational Thermal Sciences: An International Journal* 8 (4) (2016).
- [64] M. Sheikholeslami, D. Ganji, Three dimensional heat and mass transfer in a rotating system using nanofluid, *Powder Technol.* 253 (February 2014) 789–796.
- [65] M. Sheikholeslami, D.D. Ganji, Heat transfer of Cu–water nanofluid flow between parallel plates, *Powder Technol.* 235 (February 2013) 873–879.
- [66] M. Sheikholeslami, Davood Domiri Ganji, Impact of electric field on nanofluid forced convection heat transfer with considering variable properties, *J. Mol. Liq.* 229 (March 2017) 566–573.
- [67] Omid Ali Akbari, Hamid Hassanzadeh Afrouzi, Ali Marzban, Davood Toghraie, Hossein Malekzade, Abedin Arabpour, Investigation of volume fraction of nanoparticles effect and aspect ratio of the twisted tape in the tube, *J. Therm. Anal. Calorim.* (2017), <https://doi.org/10.1007/s10973-017-6372-7>.
- [68] O.A. Akbari, D. Toghraie, A. Karimipour, A. Marzban, G.R. Ahmadi, The effect of velocity and dimension of solid nanoparticles on heat transfer in non-Newtonian nanofluid, *Phys. E.* 86 (2017) 68–75.
- [69] O.A. Akbari, D. Toghraie, A. Karimipour, Impact of ribs on flow parameters and laminar heat transfer of water–aluminum oxide nanofluid with different nanoparticle volume fractions in a three-dimensional rectangular microchannel, *Adv. Mech. Eng.* 7 (11) (2015) 1–11.
- [70] O.A. Akbari, M. Goodarzi, M. RezaSafaei, M. Zarringhalam, G.R. Ahmadi, Sheikh Shabani, M. Dahari, A modified two-phase mixture model of nanofluid flow and heat transfer in 3-D curved microtube, *Adv. Powder Technol.* 27 (2016) 2175–2185.
- [71] H. Alipour, A. Karimipour, M.R. Safaei, D. Toghraie Semiromi, O.A. Akbari, Influence of T-semi attached rib on turbulent flow and heat transfer parameters of a silver-water nanofluid with different volume fractions in a three-dimensional trapezoidal microchannel, *Phys. E.* 88 (2017) 60–76.
- [72] O.A. Akbari, H. Hassanzadeh Afrouzi, A. Marzban, D. Toghraie, H. Malekzade, A. Arabpour, Investigation of volume fraction of nanoparticles effect and aspect ratio of the twisted tape in the tube, *J. Therm. Anal. Calorim.* (2017), <https://doi.org/10.1007/s10973-017-6372-7>.
- [73] M. Hemmat Esfe, M. Afrand, W.M. Yan, H. Yarmand, D. Toghraie, M. Dahari, Effects of temperature and concentration on rheological behavior of MWCNTs/SiO<sub>2</sub> (20–80)-SAE40 hybrid nano-lubricant, *Int. Commun. Heat Mass Transfer* 76 (2016) 133–138.
- [74] M. Afrand, D. Toghraie, B. Ruhani, Effects of temperature and nanoparticles concentration on rheological behavior of Fe<sub>3</sub>O<sub>4</sub>-Ag/EG hybrid nanofluid: an experimental study, *Exp. Thermal Fluid Sci.* 77 (2016) 38–44.
- [75] M. Hemmat Esfe, W.M. Yan, M. Afrand, M. Sarraf, D. Toghraie, M. Dahari, Estimation of thermal conductivity of Al<sub>2</sub>O<sub>3</sub>/water(40%)–ethylene-glycol (60%) by artificial neural network and correlation using experimental data, *Int. Commun. Heat Mass Transfer* 74 (2016) 125–128.
- [76] D. Toghraie, V.A. Chaharsoghi, M. Afrand, Measurement of thermal conductivity of ZnO–TiO<sub>2</sub>/EG hybrid nanofluid, *J. Therm. Anal. Calorim.* (2016) 1–9, <https://doi.org/10.1007/s10973-016-5436-4>.
- [77] A. Malvandi, F. Hedayati, D.D. Ganji, Thermodynamic optimization of fluid flow over an isothermal moving plate, *Alex. Eng. J.* 52 (3) (September 2013) 277–283.
- [78] D. Toghraie, S.M.B. Alempour, M. Afrand, Experimental determination of viscosity of water based magnetite nanofluid for application in heating and cooling systems, *Journal Magnetism and magnetic materials, J. Magn. Magn. Mater.* 417 (2016) 243–248.
- [79] M. Hemmat Esfe, S. Saedodin, S. Wongwises, D. Toghraie, An experimental study on the effect of diameter on thermal conductivity and dynamic viscosity of Fe/water nanofluids, *Therm Anal.* (2015), <https://doi.org/10.1007/s10973-014-4328-8>.
- [80] M. Hemmat Esfe, M. Afrand, S. Gharekhani, H. Rostamiand, D. Toghraie, M. Dahari, An experimental study on viscosity of alumina-engine oil: effects of temperature and nanoparticles concentration, *Int. Commun. Heat Mass Transfer* 76 (2016) 202–208.
- [81] O.A. Akbari, A. Karimipour, D. Toghraie Semiromi, M.R. Safaei, H. Alipour, M. Goodarzi, M. Dahari, Investigation of Rib's height effect on heat transfer and flow parameters of laminar WaterAl<sub>2</sub>O<sub>3</sub> nanofluid in a two dimensional rib-microchannel, *Appl. Math. Comput.* 290 (2016) 135–153.
- [82] A. Karimipour, H. Alipour, O.A. Akbari, D. Toghraie Semiromi, M.H. Esfe, Studying the effect of indentation on flow parameters and slow heat transfer of water–silver nanofluid with varying volume fraction in a rectangular two-dimensional microchannel, *Ind J Sci Tech* 8 (15) (July 2015) 51707.
- [83] O.A. Akbari, D. Toghraie, A. Karimipour, Numerical simulation of heat transfer and turbulent flow of water nanofluids copper oxide in rectangular microchannel with semi attached rib, *Adv. Mech. Eng.* 8 (4) (2016) 1–25.
- [84] M. Sheikholeslami, D.D. Ganji, Numerical approach for magnetic nanofluid flow in a porous cavity using CuO nanoparticles, *Mater. Des.* 120 (15) (April 2017) 382–393.
- [85] A. Moraveji, D. Toghraie, Computational fluid dynamics simulation of heat transfer and fluid flow characteristics in a vortex tube by considering the various parameters, *Int. J. Heat Mass Transf.* 432–443 (2017) (2017) 113.
- [86] O. Rezaei, O.A. Akbari, A. Marzban, D. Toghraie, F. Pourfattah, R. Mashayekhi, The numerical investigation of heat transfer and pressure drop of turbulent flow in a triangular microchannel, *Physica E: Low-dimensional Systems and Nanostructures.* 93 (2017) 179–189.
- [87] E. Keshavarz, D. Toghraie, M. Haratian, Modeling industrial scale reaction furnace using computational fluid dynamics: a case study in Ilam gas treating plant, *Appl. Therm. Eng.* 123 (2017) 277–289.
- [88] M. Sheikholeslami, Soheil Soleimani, D.D. Ganji, Effect of electric field on hydrothermal behavior of nanofluid in a complex geometry, *J. Mol. Liq.* 213 (January 2016) 153–161.

- [89] M. Sheikholeslami, M.M. Rashidi, D.D. Ganji, Numerical investigation of magnetic nanofluid forced convective heat transfer in existence of variable magnetic field using two phase model, *J. Mol. Liq.* 212 (December 2015) 117–126.
- [90] Q. Gravndyan, O.A. Akbari, D. Toghraie, A. Marzban, R. Mashayekhi, R. Karimi, F. Pourfattah, The effect of aspect ratios of rib on the heat transfer and laminar water/TiO<sub>2</sub> nanofluid flow in a two-dimensional rectangular microchannel, *J. Mol. Liq.* 236 (2017) 254–265.
- [91] M.R. Shamsi, O.A. Akbari, A. Marzban, D. Toghraie, R. Mashayekhi, Increasing heat transfer of non-Newtonian nanofluid in rectangular microchannel with triangular ribs, *Physica E: Low-dimensional Systems and Nanostructures*. 93 (2017) 167–178.
- [92] M. Sheikholeslami, D.D. Ganji, Numerical analysis of nanofluid transportation in porous media under the influence of external magnetic source, *J. Mol. Liq.* 233 (May 2017) 499–507.
- [93] S. Saffari, M. Hashemian, D. Toghraie, Dynamic Stability of Functionally Graded Nanobeam Based on Nonlocal Timoshenko Theory Considering Surface Effects, 2017, <https://doi.org/10.1016/j.physb.2017.06.029>.
- [94] O. Rezaei, O.A. Ali Akbari, A. Marzban, D. Toghraie, F. Pourfattah, R. Mashayekhi, The Numerical Investigation of Heat Transfer and Pressure Drop of Turbulent Flow in a Triangular Microchannel, 2017, <https://doi.org/10.1016/j.physe.2017.06.013>.
- [95] O. Rezaei, O.A. Ali Akbari, A. Marzban, D. Toghraie, F. Pofattah, R. Mashayekhi, The Numerical Investigation of Heat Transfer and Pressure Drop of Turbulent Flow in a Triangular Microchannel, 2015, <https://doi.org/10.1016/j.physe.2017.06.013>.
- [96] M. Siavashi, H.R.T. Bahrani, H. Saffari, Numerical investigation of flow characteristics, heat transfer and entropy generation of nanofluid flow inside an annular pipe partially or completely filled with porous media using two-phase mixture model, *Energy* 93 (2015) 2451–2466.
- [97] S. Malik, A.K. Nayak, MHD convection and entropy generation of nanofluid in a porous enclosure with sinusoidal heating, *Int. J. Heat Mass Transf.* 111 (2017) 329–345.
- [98] M. Heydari, D. Toghraie, O.A. Akbari, The effect of semi-attached and offset mid-truncated ribs and water/TiO<sub>2</sub> nanofluid on flow and heat transfer properties in a triangular microchannel, *Thermal Science and Engineering Progress*. 2 (2017) 140–150.